The current issue and full text archive of this journal is available at
www.emeraldinsight.com/0961-5539.htm

Received 21 February 2007
Revised 6 September 2007
Accepted 9 October 2007

Numerical method of lattice Boltzmann simulation for flow past a rotating circular cylinder with heat transfer

Y.Q. Zu and Y.Y. Yan
School of the Built Environment, University of Nottingham, Nottingham, UK
W.P. Shi
School of Mathematics, Jilin University, Changchun, People's Republic of China, and
L.Q. Ren
Key Laboratory of Terrain Machine Bionic Engineering, Jilin University, Changchun, People's Republic of China

Abstract

Purpose – The main objective of this work is to develop a boundary treatment in lattice Boltzmann method (LBM) for curved and moving boundaries and using this treatment to study numerically the flow around a rotating isothermal circular cylinder with/without heat transfer.

Design/methodology/approach – A multi-distribution function thermal LBM model is used to simulate the flow and heat transfer around a rotating circular cylinder. To deal with the calculations on the surface of cylinder, a novel boundary treatment is developed.

Findings – The results of simulation for flow and heat transfer around a rotating cylinder including the evolution with time of velocity field, and the lift and drag coefficients are compared with those of previous theoretical, experimental and numerical studies. Excellent agreements show that present LBM including boundary treatment can achieve accurate results of flow and heat transfer. In addition, the effects of the peripheral-to-translating-speed ratio, Reynolds number and Prandtl number on evolution of velocity and temperature fields around the cylinder are tested.

Practical implications – There is a large class of industrial processes which involve the motion of fluid passing rotating isothermal circular cylinders with/without heat transfer. Operations ranging from paper and textile making machines to glass and plastics processes are a few examples.

Originality/value – A strategy for LBM to treat curved and moving boundary with the second-order accuracy for both velocity and temperature fields is presented. This kind of boundary treatment is very easy to implement and costs less in computational time.

Keywords Fluid dynamics, Simulation, Heat transfer, Boundary layers

Paper type Research paper

International Journal of Numerical Methods for Heat & Fluid Flow
Vol. 18 No. 6, 2008
pp. 766-782

0961-5539
DOI 10.1108/09615530810885560

The work is supported by the University of Nottingham's Academic Scholarship and Siemens Industrial Turbomachinery Ltd (UK)'s case studentship. The authors would also like to thanks for the support from the International Collaboration Project from Chinese Scientific Ministry (Ref: 2005DFA00850) and Jilin University under the 985 programme.

Nomenclature

c = streaming speed, $c \equiv \delta x/\delta t$
c_s = velocity of sound
CD = drag coefficient, $CD = D/(\rho U^2 R)$
CL = lift coefficient, $CL = L/(\rho U^2 R)$
D = horizontal component of $\mathbf{F}$
$\mathbf{e}$ = discrete velocity vector
f = distribution function of density
$\mathbf{F}$ = total force acted on the solid wall
g = distribution function of temperature
h = frequency of vortex shedding
k = ratio of V to U, $k = V/U$
L = vertical component of $\mathbf{F}$
$\mathbf{n}$ = outer-normal vector of cylindrical wall
Nu = Nusselt number, $Nu = -(2R/(T_h - T_l))(\partial T/\partial \mathbf{n})_{wall}$
Pr = Prandtl number, $Pr = \nu/\gamma$
R = radius of the circular cylinder
Re = Reynolds number, $Re = 2UR/\nu$
t = time
St = Strouhal number, $St = hR/U$
T = temperature
T_l = fluid temperature at the entrance
T_h = temperature on the cylinder wall
$\mathbf{u}$ = velocity vector
u = horizontal component of $\mathbf{u}$
v = vertical component of $\mathbf{u}$
U = uniform inlet velocity of the flow field
V = peripheral velocity of the cylinder
$\mathbf{x}$ = Cartesian coordinate
x = horizontal component of $\mathbf{x}$
y = vertical component of $\mathbf{x}$

Greek symbols

α = direction number ($\alpha = 0, \ldots, 8$)
δx = time step length
δt = space step length
ϕ = scalar array
ν = kinematical viscosity
ρ = density
τ_ν = relaxation times for velocity fields
τ_c = relaxation times for temperature fields
ω = weighting coefficient
γ = thermal diffusivity
Ω = angular velocity of the circular cylinder

Subscripts and superscripts

α = direction number ($\alpha = 0, \ldots, 8$)
* = dimensionless quantities
$\sim$ = post-collision states
(eq) = equilibrium states
(neq) = nonequilibrium parts
$\langle \bullet \rangle$ = surface-averaged quantities
$\overline{\bullet}$ = period-averaged quantities
$\overline{\langle \bullet \rangle}$ = period-and-surface-averaged quantities
$\wedge$ = approximation values

1. Introduction

There is a large class of industrial processes which involve motion of fluid passing rotating isothermal circular cylinders with/without heat transfer. Operations ranging from paper and textile making machines to glass and plastics processes are a few examples.

Over the past few decades, much theoretical and experimental effort has been made to investigate isothermal flow fields past a rotating cylinder (Badr and Dennis, 1985; Bergmann *et al.*, 2006; Coutanceau and Menard, 1985; Mittal and Kumar, 2003; Nair *et al.*, 1998; Takada and Tsutahara, 1998). However, the studies, especially on numerical simulations of non-isothermal flows past a rotating cylinder are still quite limited. Therefore, the further effort is made in this paper to study numerically the flow and heat transfer from a rotating cylinder in cross-flow.

In the present study, the lattice Boltzmann method (LBM) is employed to simulate such flow across rotating cylinder with heat transfer. Unlike, conventional CFD simulations which are mainly based on a direct numerical approximation to the macroscopic *N-S* equation, the LBM is to construct simplified kinetic models that incorporate the essential physics of microscopic or mesoscopic processes so that the macroscopic averaged properties obey the desired macroscopic equations (Chen and Doolen, 1998). The attractive features, including the simplicity of programming, the high efficiency on handling interactions between the fluid and wall with complicated geometry, etc. make the LBM a better choice for the present simulation.

In general, the existing LBM models for dealing with thermal fluid flows can basically be divided into two distinct categories, namely: the multi-speed models (Alexander *et al.*, 1993; Teixeira *et al.*, 2000; Watari and Tsutahara, 2004) and the multi-distribution function models (Barrios *et al.*, 2005; Guo *et al.*, 2002a; He *et al.*, 1998; Peng *et al.*, 2003; Shi *et al.*, 2004). In the multi-speed models, only the density distribution function is used; to obtain the macroscopic energy equation, additional discrete velocities are introduced; and the equilibrium distributions usually include higher order velocity terms. In the multi-distribution function models, in addition to the original density distribution function, a distribution function for temperature is also introduced. This kind of models can effectively overcome two limitations of the multi-speed models, namely, severe numerical instability and narrow range of temperature variation (He *et al.*, 1998). Therefore, in the present study and simulation, a multi-distribution function model is chosen as the numerical scheme.

To handle the moving curved boundary of temperature field, an extrapolation method based on the idea of Guo *et al.* (2002b) will be extended. The method combined with the velocity boundary treatment presented by Mei *et al.* (2002) can satisfy the second-order accuracy for both velocity and temperature on the curved wall.

2. Lattice Boltzmann equations

A two-dimensional nine-velocity (D2Q9) LBM model, as shown in Figure 1, with multiple distribution functions (Barrios *et al.*, 2005; Guo *et al.*, 2002a) is introduced to simulate incompressible viscous thermal flows:

$$f_\alpha(\mathbf{x}+\mathbf{e}_\alpha\delta t, t+\delta t) - f_\alpha(\mathbf{x},t) = \frac{\left[f_\alpha^{(\mathrm{eq})}(\mathbf{x},t) - f_\alpha(\mathbf{x},t)\right]}{\tau_\nu}; \tag{1}$$

$$g_\alpha(\mathbf{x}+\mathbf{e}_\alpha\delta t, t+\delta t) - g_\alpha(\mathbf{x},t) = \frac{\left[g_\alpha^{(\mathrm{eq})}(\mathbf{x},t) - g_\alpha(\mathbf{x},t)\right]}{\tau_c}. \tag{2}$$

where $f_\alpha(\mathbf{x},t)$ and $g_\alpha(\mathbf{x},t)$ are, respectively, the density and temperature distribution functions along the αth direction; $f_\alpha^{(\mathrm{eq})}(\mathbf{x},t)$ and $g_\alpha^{(\mathrm{eq})}(\mathbf{x},t)$ are their corresponding equilibrium states, where:

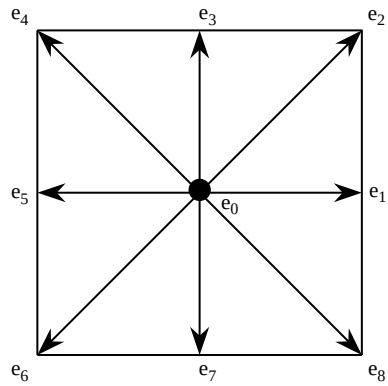

Figure 1.
The discrete velocity set of D2Q9 model

$$f_\alpha^{(\mathrm{eq})}(\mathbf{x},t)=\omega_\alpha\rho\left[1+\frac{3}{c^2}(\mathbf{e}_\alpha\cdot\mathbf{u})+\frac{9}{2c^2}(\mathbf{e}_\alpha\cdot\mathbf{u})^2-\frac{3}{2c^2}\mathbf{u}^2\right]; \tag{3}$$

$$g_\alpha^{(\mathrm{eq})}(\mathbf{x},t)=\omega_\alpha T\left[1+\frac{3}{c^2}\mathbf{e}_\alpha\cdot\mathbf{u}\right]; \tag{4}$$

$$\mathbf{e}_\alpha=\begin{cases}0, & \alpha=0\\ (\cos[(\alpha-1)\pi/4],\ \sin[(\alpha-1)\pi/4])c, & \alpha=1,3,5,7\\ \sqrt{2}(\cos[(\alpha-1)\pi/4],\ \sin[(\alpha-1)\pi/4])c, & \alpha=2,4,6,8\end{cases}; \tag{5}$$

$$\omega_\alpha=\begin{cases}4/9, & \alpha=0\\ 1/9, & \alpha=1,3,5,7\\ 1/36, & \alpha=2,4,6,8\end{cases}, \tag{6}$$

where $c_\mathrm{s}=c/\sqrt{3}$ is the speed of sound, other parameters such as $\mathbf{u}$, ρ, T, ν and γ are evaluated as:

$$\rho=\sum_\alpha f_\alpha,\quad \rho\mathbf{u}=\sum_\alpha\mathbf{e}_\alpha f_\alpha,\quad T=\sum_\alpha g_\alpha,\quad \nu=\frac{\tau_\nu-0.5}{c_\mathrm{s}^2\delta t},\quad \gamma=\frac{\tau_c-0.5}{c_\mathrm{s}^2\delta t}. \tag{7}$$

Under the incompressible flow limit (i.e. the Mach number $Ma=|\mathbf{u}|/c_\mathrm{s}\ll 1$), through the Chapman-Enskog expansion, the mass, momentum and energy equations can be derived from the D2Q9 model as follows (Guo *et al.*, 2002a; Yu *et al.*, 2003):

$$\nabla\cdot\mathbf{u}=0; \tag{8}$$

$$\frac{\partial\mathbf{u}}{\partial t}+(\mathbf{u}\cdot\nabla)\mathbf{u}=-\frac{1}{\rho}\nabla p+\nu\nabla^2\mathbf{u}; \tag{9}$$

$$\frac{\partial T}{\partial t}+\nabla\cdot(\mathbf{u}T)=\gamma\nabla^2T. \tag{10}$$

3. Curved boundary treatment in LBM

Equations (1) and (2) can be computed by the following two steps, i.e. collision and streaming:

$$\text{Collision step}:\tilde{f}_\alpha(\mathbf{x},t)=f_\alpha(\mathbf{x},t)-\frac{\left[f_\alpha(\mathbf{x},t)-f_\alpha^{(\mathrm{eq})}(\mathbf{x},t)\right]}{\tau_\nu}; \tag{11a}$$

$$\tilde{g}_\alpha(\mathbf{x},t)=g_\alpha(\mathbf{x},t)-\frac{\left[g_\alpha(\mathbf{x},t)-g_\alpha^{(\mathrm{eq})}(\mathbf{x},t)\right]}{\tau_c}; \tag{11b}$$

$$\text{Streaming step}:f_\alpha(\mathbf{x}+\mathbf{e}_\alpha\delta t,t+\delta t)=\tilde{f}_\alpha(\mathbf{x},t); \tag{12a}$$

$$g_\alpha(\mathbf{x}+\mathbf{e}_\alpha\delta t,t+\delta t)=\tilde{g}_\alpha(\mathbf{x},t). \tag{12b}$$

As shown in Figure 2, an arbitrary curved wall (the dashed line) separates the solid region from the fluid region. The black solid circles ●, the open circles ˆ and the grey solid circles ○ denote the intersections of the boundary with various lattice links ($\mathbf{x}_w$), the boundary nodes in the fluid region ($\mathbf{x}_f$), and those in the solid region ($\mathbf{x}_b$), respectively. Obviously, $\tilde{f}_{\bar{\alpha}}(\mathbf{x}_b, t)$ and $\tilde{g}_{\bar{\alpha}}(\mathbf{x}_b, t)$ are needed to perform the streaming step at the fluid node $\mathbf{x}_f$.

The fraction of an intersected link in the fluid region, Δ, can be defined as:

$$\Delta = \frac{|\mathbf{x}_f - \mathbf{x}_w|}{|\mathbf{x}_f - \mathbf{x}_b|}. \tag{13}$$

In LBM, the bounce-back scheme was usually applied at the wall boundaries to obtained no-slip velocity condition. The scheme comes from the idea that a particle distribution streaming to a wall will be bounced back at the next time-step. Accordingly, the interacting force between the fluid and wall can be approximated by the momentum change of the particles neighbouring the wall over a time step (Mei *et al.*, 2002). This feature enables the boundary treatment in LBM to be very easy. It is well known that the bounce-back boundary condition satisfies a no-slip velocity boundary condition with second-order accuracy when $\Delta = 1/2$. Thermal boundary conditions can be implemented in a similar way, which can achieve second-order accuracy too. However, this method can only be used to treat some simple boundaries of straight line parallel to the lattice grid. For a curved boundary, simply placing boundary at $\Delta = 1/2$ will factitiously change the boundary geometry and degrade the accuracy of the velocity and temperature fields. In this section, a boundary treatment with second-order accuracy for both velocity and temperature boundaries will be introduced. For the velocity field, an accurate curved boundary treatment given by Mei *et al.* (2002) will be employed. Meanwhile, based on the existing idea of extrapolation of velocity boundary (Guo *et al.*, 2002b), a method with second-order accuracy to handle the boundary of temperature fields will be presented.

As we know, for velocity field around an arbitrary shaped body, it is difficult to obtain analytical solutions. Nevertheless, a substantial evidence has show that the bounce-back boundary conditions combined with interpolations including the one-half

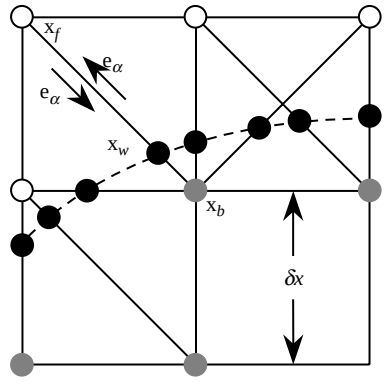

Figure 2.
The layout of regularly spaced lattices and curved wall boundary

grid spacing correction at boundaries, are in fact of second-order accurate and thus ca-pable of handling curved boundaries (Mei *et al.*, 2002; Yu *et al.*, 2003). $\tilde{f}_{\bar{\alpha}}(\mathbf{x}_b, t)$ can be constructed based upon some know information in the surrounding:

$$\begin{aligned}\tilde{f}_{\bar{\alpha}}(\mathbf{x}_b, t) = \tilde{f}_{\alpha}(\mathbf{x}_f, t) - \chi\left[\tilde{f}_{\alpha}(\mathbf{x}_f, t) - f_{\alpha}^{(\mathrm{eq})}(\mathbf{x}_f, t)\right] \\ + \omega_{\alpha}\rho(\mathbf{x}_f, t)\frac{3}{c^2}\mathbf{e}_{\alpha}\cdot[\chi(\mathbf{u}_{bf} - \mathbf{u}_f) - 2\mathbf{u}_w];\end{aligned} \tag{14}$$

where:

$$\mathbf{u}_{bf} = \mathbf{u}_{ff} = \mathbf{u}(\mathbf{x}_{ff}, t), \quad \chi = \frac{2\Delta - 1}{\tau - 2}, \quad \text{if } 0 \le \Delta < \frac{1}{2}; \tag{15a}$$

$$\mathbf{u}_{bf} = \frac{1}{2\Delta}(2\Delta - 3)\mathbf{u}_f + \frac{3}{2\Delta}\mathbf{u}_w, \quad \chi = \frac{2\Delta - 1}{\tau - (1/2)}, \quad \text{if } \frac{1}{2} \le \Delta < 1. \tag{15b}$$

In the above:

$$\mathbf{e}_{\bar{\alpha}} \equiv -\mathbf{e}_{\alpha}, \ \ \mathbf{x}_{ff} = \mathbf{x}_f + \mathbf{e}_{\bar{\alpha}}\delta_t, \ \ \mathbf{u}_f \equiv \mathbf{u}(x_f, t), \ \ \mathbf{u}_w \equiv \mathbf{u}(\mathbf{x}_w, t);$$

where $\mathbf{u}_{bf}$ is the imaginary velocity for interpolations, and χ is weight factor.

To implement the curved boundary treatment for temperature, the non-equilibrium parts of temperature distribution function, $g_{\alpha}^{(\mathrm{neq})}(\mathbf{x}, t) = g_{\alpha}(\mathbf{x}, t) - g_{\alpha}^{(\mathrm{eq})}(\mathbf{x}, t)$, is introduced. Let the temperature at $\mathbf{x}_w$, $\mathbf{x}_f$ and $\mathbf{x}_{ff}$ be T_w, T_f and T_{ff}, respectively. Then, $\tilde{g}_{\bar{\alpha}}(\mathbf{x}_b, t)$ can be approximated by an extrapolation method with second-order accuracy:

$$\tilde{g}_{\bar{\alpha}}(\mathbf{x}_b, t) = \frac{1 - 1}{\tau_c}g_{\bar{\alpha}}^{(\mathrm{neq})}(\mathbf{x}_b, t) + \omega_{\bar{\alpha}}\hat{T}_b\left[1 + 3\mathbf{e}_{\bar{\alpha}}\cdot\frac{\hat{\mathbf{u}}_b}{c^2}\right]; \tag{16}$$

$$\left.\begin{aligned} g_{\bar{\alpha}}^{(\mathrm{neq})}(\mathbf{x}_b, t) &= g_{\bar{\alpha}}^{(\mathrm{neq})}(\mathbf{x}_f, t) \\ \hat{\mathbf{u}}_b &= [\mathbf{u}_w + (\Delta - 1)\mathbf{u}_f]/\Delta \\ \hat{T}_b &= [T_w + (\Delta - 1)T_f]/\Delta \end{aligned}\right\}, \quad \text{if } \Delta \ge 0.75; \tag{17a}$$

$$\left.\begin{aligned} g_{\bar{\alpha}}^{(\mathrm{neq})}(\mathbf{x}_b, t) &= \Delta g_{\bar{\alpha}}^{(\mathrm{neq})}(\mathbf{x}_f, t) + (1 - \Delta)g_{\bar{\alpha}}^{(\mathrm{neq})}(\mathbf{x}_{ff}, t) \\ \hat{\mathbf{u}}_b &= \mathbf{u}_w + (\Delta - 1)\mathbf{u}_f + [2\mathbf{u}_w + (\Delta - 1)\mathbf{u}_{ff}](1 - \Delta)/(1 + \Delta) \\ \hat{T}_b &= T_w + (\Delta - 1)T_f + [2T_w + (\Delta - 1)T_{ff}](1 - \Delta)/(1 + \Delta) \end{aligned}\right\}, \tag{17b}$$

$$\text{if } \Delta < 0.75.$$

Consequently, on the temperature boundary, the second-order accuracy can be satisfied by using $\tilde{h}_{\bar{\alpha}}(\mathbf{x}_b, t)$ to approximate $\tilde{g}_{\bar{\alpha}}(\mathbf{x}_b, t)$.

It should be noted that the present boundary treatment for velocity and temperature fields inherits the basic idea of the bounce back scheme. Therefore, it is easy to be implemented and costs less in computational time.

In the present simulation, a momentum-exchange method (Mei *et al.*, 2002) is employed to evaluate the force on the circular cylinder surface. In order to implement

the method efficiently, a scalar array $\phi(i, j)$ is employed. $\phi(i, j) = 0$ refers to that the lattice location (i, j) is occupied by fluid; For those lattice nodes inside the solid body, $\phi(i, j) = 1$ is given. For a given boundary node $\mathbf{x}_b$ inside the solid region, the momentum-exchange with all possible neighboring fluid nodes over a time step is given by:

$$\sum_{\alpha \neq 0} \mathbf{e}_\alpha [\tilde{f}_\alpha(\mathbf{x}_b, t) + \tilde{f}_{\bar{\alpha}}(\mathbf{x}_b + \mathbf{e}_{\bar{\alpha}}\delta_t, t)][1 - \phi(\mathbf{x}_b + \mathbf{e}_{\bar{\alpha}}\delta_t)]. \tag{18}$$

The total force acted on the solid body by fluid can be obtained by summing the contribution over all boundary nodes $\mathbf{x}_b$ belonging to the body, i.e.:

$$\mathbf{F} = \sum_{\text{all } xb} \sum \mathbf{e}_\alpha [\tilde{f}_\alpha(\mathbf{x}_b, t) + \tilde{f}_{\bar{\alpha}}(\mathbf{x}_b + \mathbf{e}_{\bar{\alpha}}\delta_t, t)][1 - \phi(\mathbf{x}_b + \mathbf{e}_{\bar{\alpha}}\delta_t)]. \tag{19}$$

In the momentum-exchange method, force $\mathbf{F}$ is evaluated after the collision step and that the value of $\tilde{f}_{\bar{\alpha}}$ on the boundary given by equation (14) is also evaluated.

4. Numerical simulation

As shown in Figure 3, the velocity and temperature fields around a rotating isothermal circular cylinder of radius R are numerical simulated in the (x, y)-plane by the LBM. The coordinates x and y are taken, respectively, to be measured along the horizontal and vertical directions with the origin at the center of the circular cylinder. The flow-field considered here is in a rectangular domain. At the entrance, i.e. the left hand side boundary, fluid with the constant temperature T_l is injected into the flow domain with constant uniform velocity U in x-direction. Meanwhile, a free outflow boundary is set on the right hand side of the domain. The upper and lower boundaries are set as free-slip velocity and heat insulated boundaries. The four sides of the domain should be placed far enough from the center of the cylinder in order to eliminate the effect of boundaries. In the simulations, the boundaries at upstream, downstream and two other

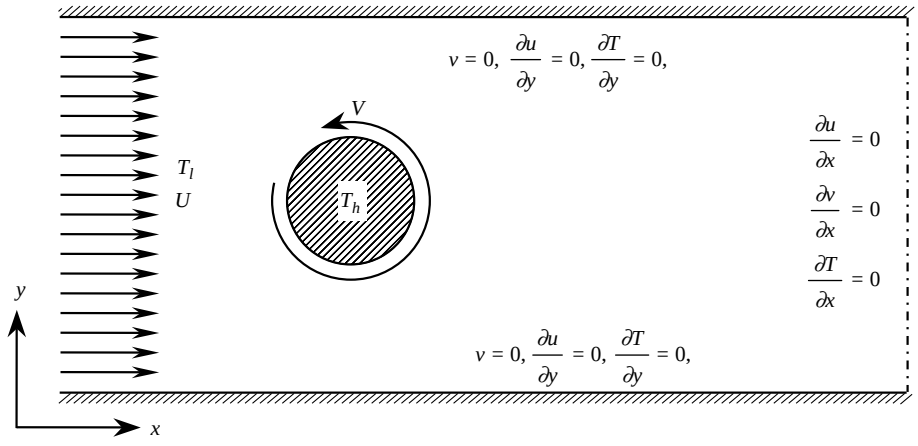

Figure 3.
The model of flow and heat transfer around a single rotating cylinder

sides are put as 6.6R, 12.07R and 8.07R, respectively, away from the center of the cylinder. Initially, the flow field is given by $u(x, y) = U$, $v(x, y) = 0$ with uniform temperature T_l, and the cylinder is stationary with temperature T_h. At the next moment, the cylinder suddenly starts to rotate with an angular velocity Ω, and the surface temperature is kept at constant T_h. In the simulations, in order to regard the fluid as incompressible, the flow velocity must be much smaller than the speed of sound. Therefore, the inflow velocity U is set at 0.01 for $Re = 200$ and 0.005 for $Re = 500$ and 1,000, respectively. Parameter k is introduced to define the ratio of the peripheral velocity $V = \Omega R$ to U, i.e. $k = V/U$. For all cases, we have $T_h = 40$, $T_l = 20$, $\rho = 6$.

By using the dimensionless quantities, the results obtained by the present method can be compared with those by other theoretical, numerical and experimental methods. Thus, velocity, displacement, time and temperature are normalized using the following relations:

$$u^* = \frac{u}{U}, \quad v^* = \frac{v}{U}, \quad x^* = \frac{x}{R}, \quad y^* = \frac{y}{R}, \quad t^* = \frac{Ut}{R}, \quad T^* = \frac{T - T_l}{T_h - T_l}. \tag{20}$$

5. Results and discussion

In this section, the velocity and temperature fields and also the force acting on the rotating cylinder are computed by the present LBM and compared with the theoretical, experimental and computational results reported by available literatures.

To ensure the numerical results obtained to be grid-independent, the sensitivities of grid number and distribution are tested. Table I shows the effects of grid size on the Strouhal number, period-averaged drag and lift coefficient, and the period-and-surface-averaged Nusselt number at $Re = 200$, $\alpha = 0.5$ and $Pr = 0.5$. In Table I, M is the number of grid point in horizontal direction, N is the number in vertically direction. For example, for $R = 15$, the satisfactory solutions can be obtained with grid distribution $M \times N = 280 \times 242$.

For the case of $Re = 200$ and $k = 0.5$, Figure 4 shows time development of wake flow pattern for the values of t^* up to 12.0. The left and right columns in the figure show the streamlines obtained by present method and those by Badr and Dennis (1985) using the finite difference method (FDM), respectively. An excellent agreement between both columns in terms of the formation of a Karman vortex street is shown.

To evaluate the consistency of the experimental and the present numerical results, the distributions of velocity components on positive x-axis are compared at several moments. Figure 5 shows the evolution with time of u^* and v^* on positive x-axis. They may be compared with Figure 17 of the paper by Coutanceau and Menard (1985) which

R	Mesh ($M \times N$)	St	$\overline{\mathrm{CD}}$	$\overline{\mathrm{CL}}$	$\overline{\langle Nu \rangle}$
6	112 × 97	0.09416	1.207	−1.258	5.999
10	187 × 161	0.1079	1.439	−1.308	6.211
15	280 × 242	0.1094	1.505	−1.331	6.237
20	373 × 323	0.1095	1.505	−1.332	6.239

Table I. Effects of grid size at $Re = 200$, $\alpha = 0.5$ and $Pr = 0.5$

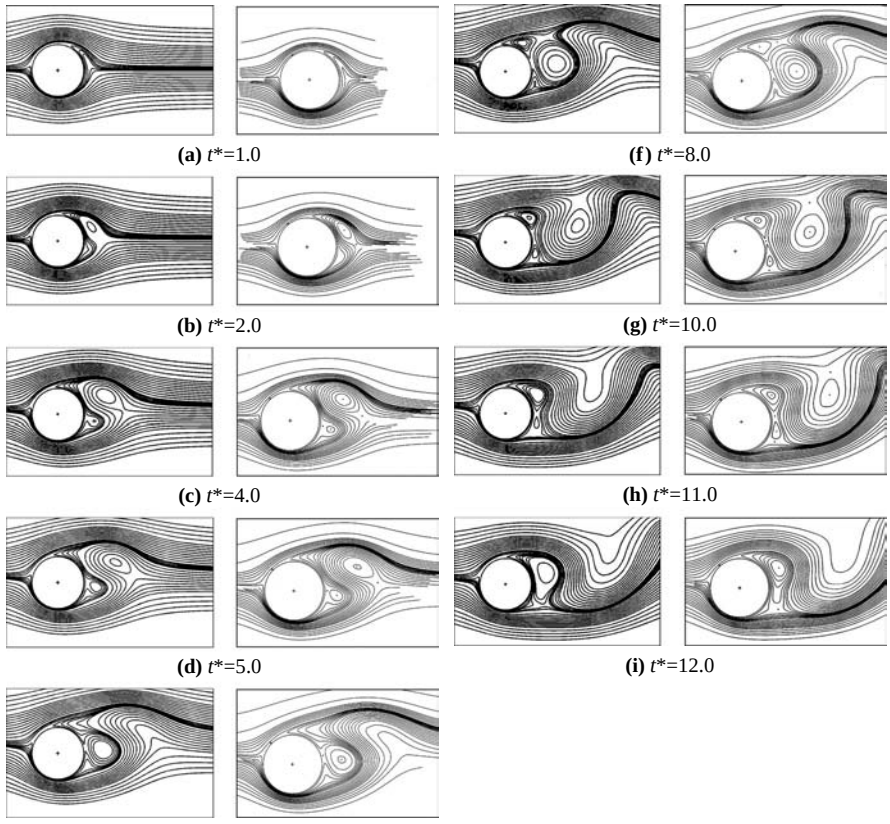

Figure 4.
(a)-(e): Caption overleaf; (f)-(i) evolution of velocity field for $Re = 200$, $k = 0.5$

Notes: Left – by the present computation; right – Badr and Dennis (1985) using FDM

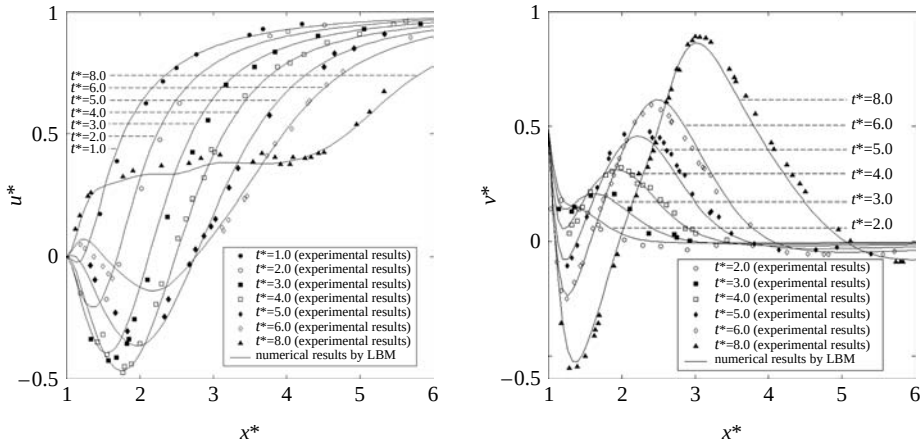

Figure 5.
Velocity profiles on x-axis for $Re = 200$, $k = 0.5$

(a) u^* on the positive x-axis

(b) v^* on the positive x-axis

indicate a good measure of quantitative agreement. Some representative points taken from the experimental study (Coutanceau and Menard, 1985) are shown in Figure 5 to illustrate the degree of the quantitative comparison.

Figure 6 shows the streamlines for the case of $Re = 200$, $k = 1.0$ by the present calculation; and a comparison with those of Badr and Dennis (1985) by FDM and the experimental visualization by Coutanceau and Menard (1985). Basically, good

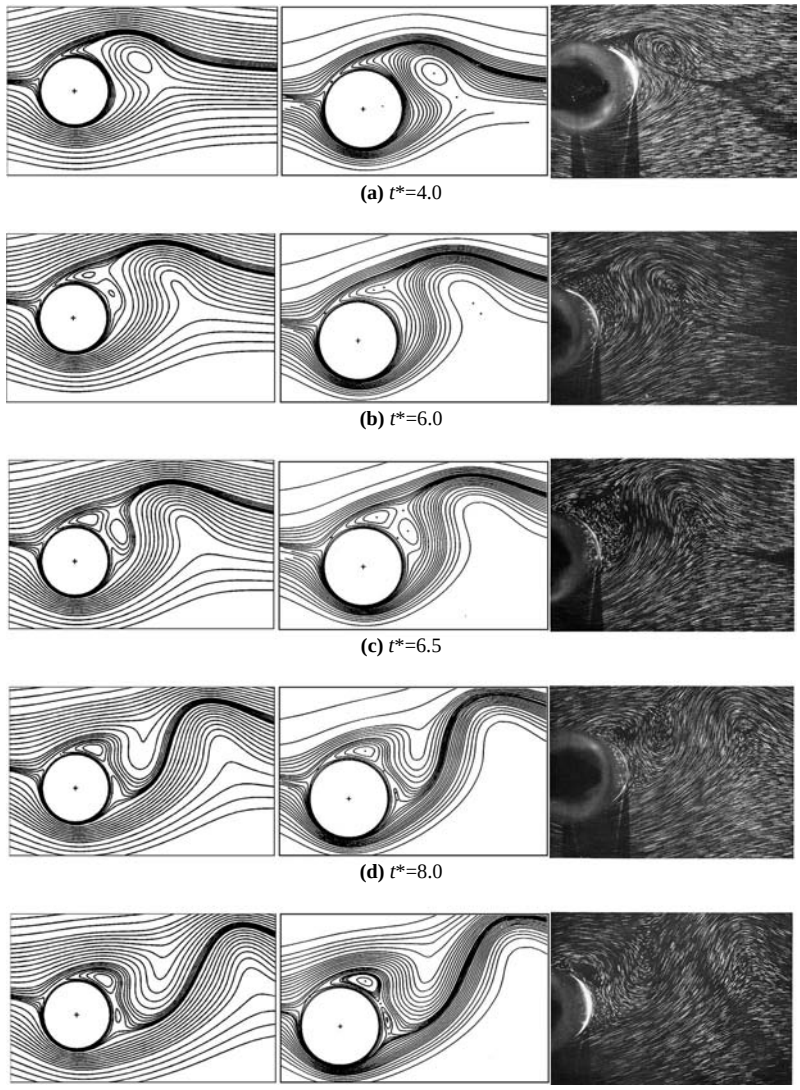

Notes: Left – by the present computation; middle – Badr and Dennis (1985) using FDM; right – experiment of Coutanceau and Menard (1985)

Figure 6.
Evolution of velocity field for $Re = 200$, $k = 1.0$

agreements can be identified except the streamlines at $t^* = 6.0$. At this moment, as shown in Figure 6(b), the streamline shows that two vortices which do not appear in the corresponding plot by FDM have been formed over the surface of the circular cylinder. In order to test which result is more accurate, two numerical results at $t^* = 6.0$ are compared, respectively, with the corresponding experimental result of Coutanceau and Menard (1985). The comparison shows that two vortices appearing in the present simulation are correct, as it was observed by the experiment when $t^* = 6.0$. This demonstrates that the present simulation based on the LBM is more realistic than that by FDM in reproducing the flow details.

At $Re = 500$, the force acting on the rotating cylinder with parameter $k = 0.1$, 0.5 and 1.0 is examined, respectively. Under the condition that t^* is small enough, Badr and Dennis (1985) have presented an approximate analytical solution for the lift coefficient which can be expressed as:

$$\mathrm{CL} = -k\left[\left(2.8996\pi - \frac{8}{3}\,\pi^{-1/2}\right)\left(\frac{2t^*}{Re}\right)^{1/2} + 5.5688\pi\left(\frac{t^*}{Re}\right)\right]. \tag{21}$$

In Figure 7(a), the variation of lift coefficient CL with time for each parameter k is shown and compared with the approximate analytical solution. The comparison shows that the approximate analytical values are indeed suitable only for an early stage of flow evolution. Moreover, it is observed that the increase of parameter k can result in a reduction of time range when an approximate analytical solution is valid. The time developments of lift coefficients for $k = 0.5$ and 1.0 are also compared with those reported numerical investigation by Takada and Tsutahara (1998), in which the evolution of isothermal flow around a suddenly rotating circular cylinder is simulated by a 2D seven-velocity LBM model. As shown in Figure 7(b), the life coefficients obtained by the latter oscillation with large amplitude, especially at an early stage of the flow evolution. In our opinion, this kind of unphysical oscillation may be caused by the lack of accuracy on the boundary. Since the boundary for the cylinder in Takada and Tsutahara's simulation was not located on a pure circle but on a polygon,

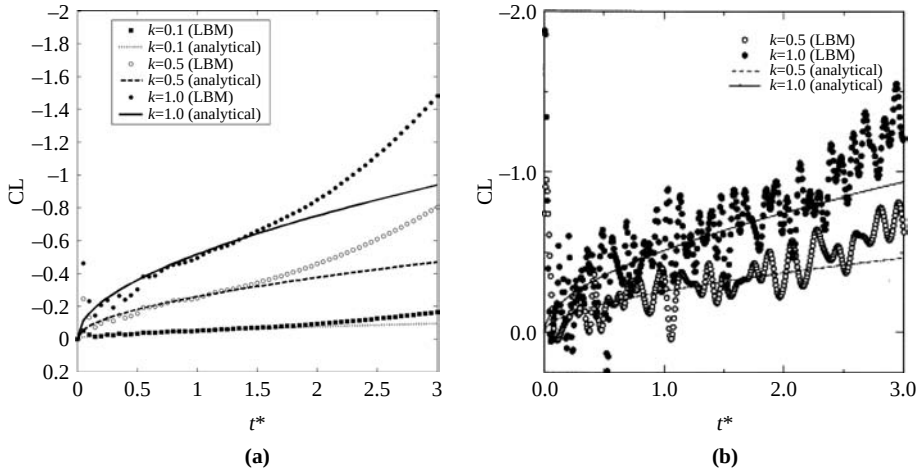

Figure 7.
The variation with time of lift coefficient for $Re = 500$: (a) computed by the present method; (b) computed by Takada and Tsutahara (1998)

the cylinder must occupy more lattice units so that the polygon may approach a circle. This kind of treatment has factitiously changed the real geometry of the boundary and therefore led to a reduction in computational accuracy. The comparison shows that the present method for dealing with curved boundary can overcome the limitation mentioned above so that is more accurate.

To further check the accuracy of the present method, the present time-averaged values of drag coefficient are compared with those obtained by Badr and Dennis (1985) using FDM (Table II) showing good consistency.

Figure 8 shows the evolution of drag and lift coefficients under the same Reynolds number 200 to examine the effects of k on the force acting on the cylinder surface. Obviously, both the drag and lift coefficients can reach the periodic state with time development if the time is long enough. Moreover, the period-averaged lift coefficients, at -0.2669, -1.331 and -2.699 for $k = 0.1$, 0.5 and 1.0, respectively, are all less than zero since the anticlockwise rotation of the cylinder. In addition, the period-averaged drag coefficients are 1.553, 1.505 and 1.349 for $k = 0.1$, 0.5 and 1.0, respectively; this

α	$\overline{CD'}$ (present)	Badr and Dennis (1985)
0.5	1.3943	1.42
1.0	1.7689	1.78

Note: Comparison of the present time-averaged values of drag coefficient from $t^* = 3$ to $t^* = 4$ for $\alpha = 0.5$ and 1.0

Table II.

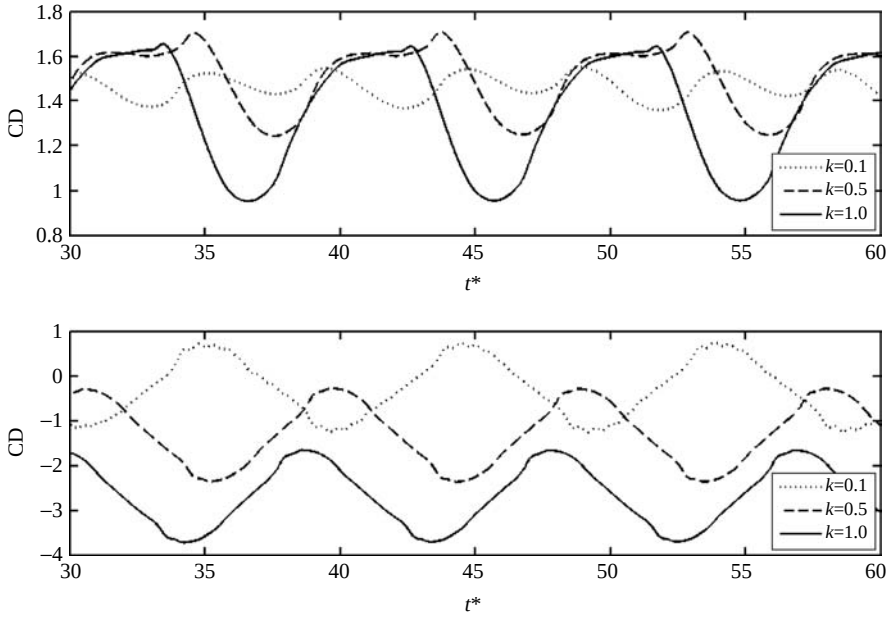

Figure 8.
The variation with time of drag and lift coefficients for $Re = 200$

indicates that the increase of k from 0.1 to 1.0 results in a decrease of period-averaged drag coefficient.

To analysis the relationship between the velocity field and temperature distributions, Figure 9 shows the evolution of temperature contours and corresponding velocity streamlines for $Re = 200$, $k = 0.5$ and $Pr = 1.0$. It can be noted from Figure 9 that an impulsive start of the cylinder leads to a generation of the initial thermal boundary layer near the surface of the isotheral cylinder; moreover, the temperature contours are almost in parallel with the cylinder wall. With time marching, the thickness of thermal boundary layer experiences a magnification everywhere. However, at the same time, the crossflow conveys more and more heat from the front to the rear of the cylinder so that the extension of thermal boundary layer is deeper at the rear than it in the front. This phenomenon becomes more evident a larger t^*. Obviously, the warming up of the boundary layer at the rear of the cylinder results in a decrease of heat flux there. It is observed that vortex shedding plays an important role in downstream heat transfer downstream. In Figure 9, with time marching, the vortices generated at the rear of the cylinder grow in size and shed into the flow stream enhancing heat transfer. As a result, high temperatures concentrate in the regions where streamlines have large curvatures caused by the opened vortices (Figure 9(g)-(j)).

Now, let us consider more precisely of what the effect of k on local heat transfer coefficient (the Nusselt number). Considering that the flow can reach a periodic state when t^* is large enough, the period-averaged values of Nusselt number distributions at $Re = 200$, $Pr = 0.5$, $\theta \in [0°, 360°]$ with $k = 0.0, 0.5, 1.0$, respectively, are plotted in polar coordinates as shown in Figure 10. Where, the angle θ is equal to zero degree at the rearmost point of the cylinder and increases anticlockwise. For $k = 0$, it can be seen clearly that the distribution curve is strictly symmetrical with respect to $\theta = 0°$, and that the maximum Nusselt number appears at $\theta = 180°$, i.e. the foremost point of the cylinder. Moreover, it is noted that for all values of k, the heat transfer coefficient on the front side is much higher than that on the back side and also each curve of Nusselt number distribution has two local minimum and two local maximum points. The overall tendency of these points with local extrema is to migrate along the surface of cylinder anticlockwise with k.

At $Re = 200$, the period-and-surface-averaged Nusselt number, i.e. $\overline{\langle Nu \rangle}$, is calculated for $Pr = 0.5$ and 1.0 and with different value of k, respectively. The results are shown in Figure 11. It is noted that an increase in parameter k results in an evident decrease in $\overline{\langle Nu \rangle}$. In addition, Figure 12 shows the variation of period-and-surface-averaged Nusselt number with Reynolds and Prandtl numbers at $k = 0.5$. Obviously, Nusselt number increases with Reynolds and Prandtl numbers.

6. Conclusion

By applying a multi-distribution function LBM model and meanwhile presenting a boundary treatment of moving curved boundary with second-order accuracy for velocity and temperature fields, the flow past a rotating isothermal circular cylinder is simulated numerically. The results of simulation including the evolution with time of velocity field, and the lift and drag coefficients agree well with those of previous theoretical, experimental and numerical studies and show that the present method of LBM can accurately simulate this type of flow problems of rotating cylinders with convective heat transfer. It is found that a higher Nusselt number can be obtained by either decreasing the velocity ratio of rotating to inflow or increasing Reynolds and Prandtl numbers.

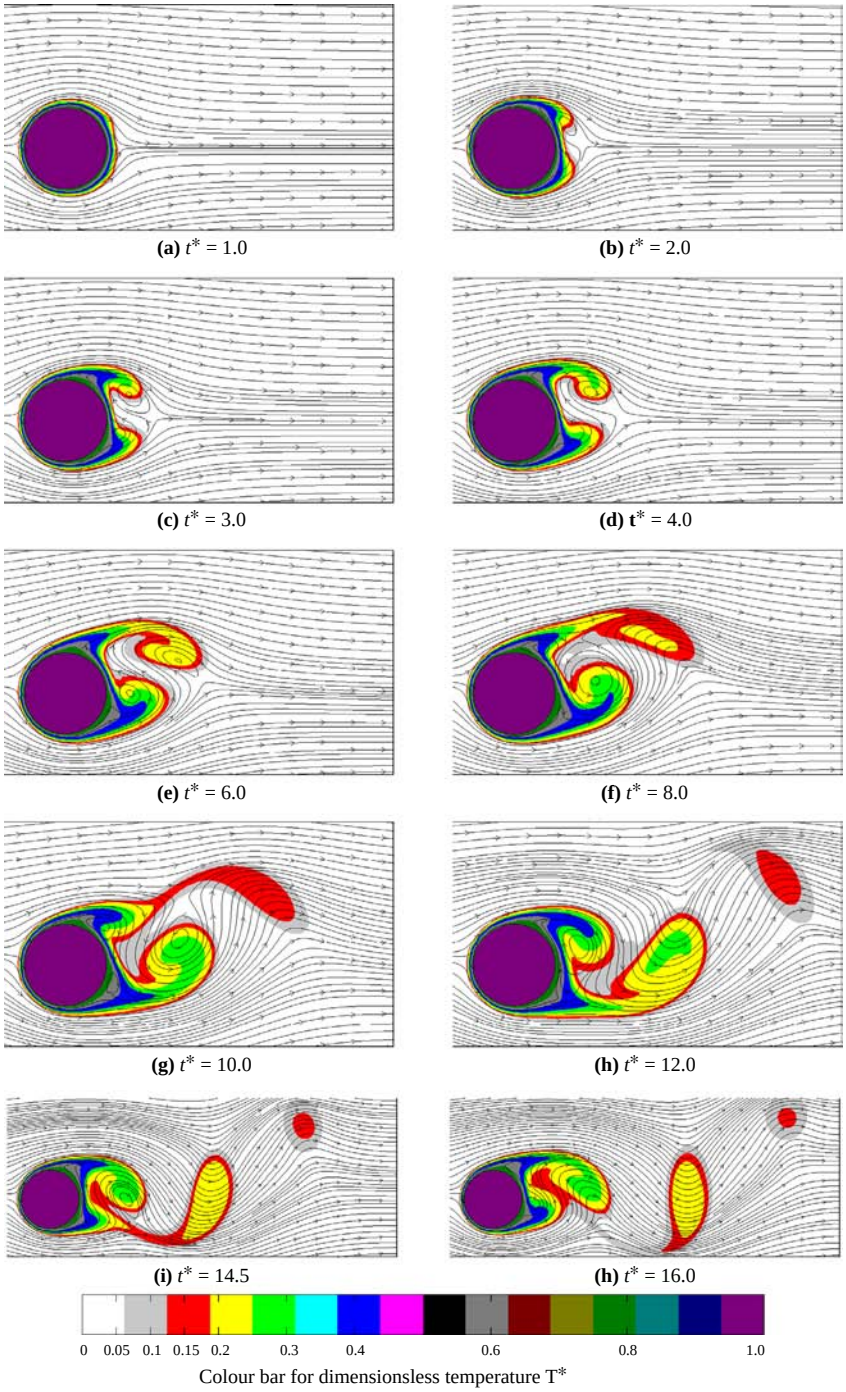

Figure 9.
Evolution of velocity streamlines and temperature contours for $Re = 200$, $k = 0.5$, $Pr = 1.0$

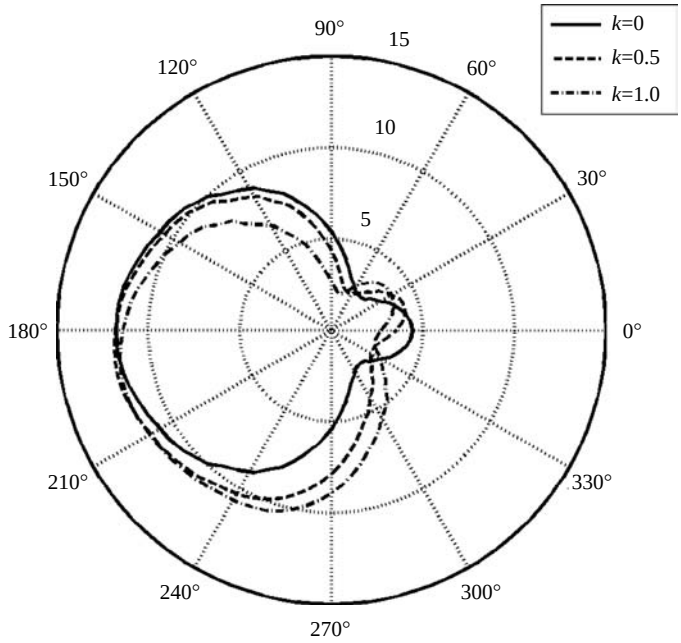

Figure 10.
Global distribution of period-average Nusselt number along the cylinder surface for $Re = 200$, $Pr = 0.5$ with different k

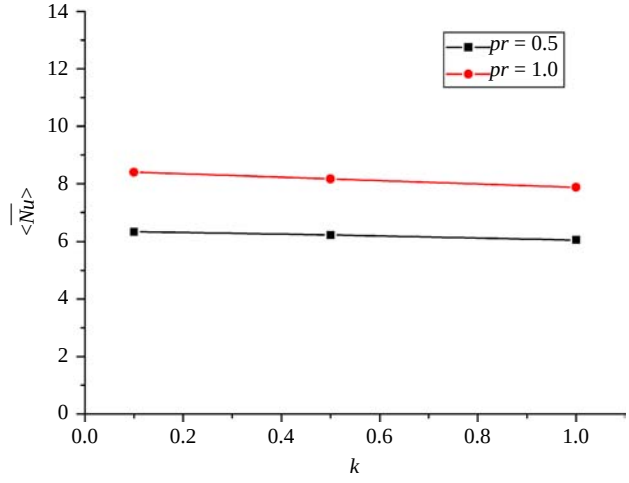

Figure 11.
Variation of period-and-surface-average Nusselt number with k at $Re = 200$, $Pr = 0.5$ and 1.0

LBM boundary treatment presented in this paper is basically easy and costs less computational time. However, the calculation for the whole computational domain in the present simulation is relatively time consuming due to the application of uniform gird. To improve the efficiency of computation, a stable LBM with non-uniform mesh should be proposed, which will be involved in our further work.

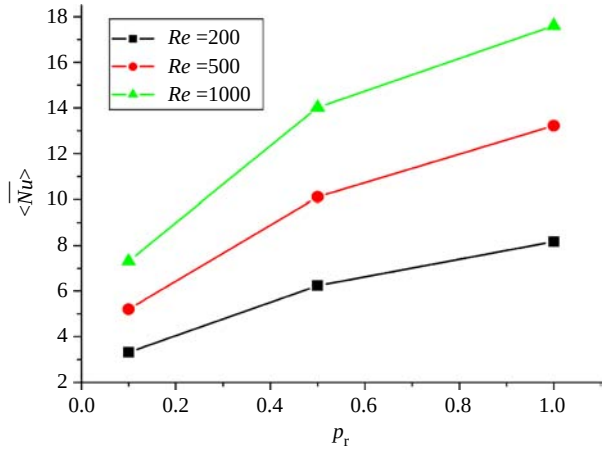

Figure 12.
Variation of period-and-surface-average Nusselt number with Pr at $k = 0.5$ and $Re = 200, 500, 1{,}000$

References

Alexander, F.J., Chen, S. and Sterling, J.D. (1993), "Lattice Boltzmann thermohydrodynamics", *Phys. Rev. E*, Vol. 47 No. 4, pp. R2249-52.

Badr, H.M. and Dennis, S.C.R. (1985), "Time-dependent viscous flow past an impulsively started rotating and translating circular cylinder", *J. Fluid Mech.*, Vol. 158, pp. 447-88.

Barrios, G., Rechtman, R., Rojas, J. and Tovar, R. (2005), "The lattice Boltzmann equation for natural convection in a two-dimensional cavity with a partially heated wall", *J. Fluid Mech.*, Vol. 522, pp. 91-100.

Bergmann, M., Cordier, L. and Brancher, J.P. (2006), "On the generation of a reverse von Karman street for the controlled cylinder wake in the laminar regime", *Phys. Fluids*, Vol. 18 No. 2, p. 028101.

Chen, S. and Doolen, G.D. (1998), "Lattice Boltzmann method for fluid flows", *Ann. Rev. Fluid Mech.*, Vol. 30, pp. 329-64.

Coutanceau, M. and Menard, C. (1985), "Influence of rotation on the near-wake development behind an impulsively started circular cylinder", *J. Fluid Mech.*, Vol. 158, pp. 399-466.

Guo, Z.L., Shi, B.C. and Zheng, C.G. (2002a), "A coupled lattice BGK model for the Boussinesq equations", *Int. J. Numer. Methods Fluids*, Vol. 39 No. 4, pp. 325-42.

Guo, Z.L., Zheng, C.G. and Shi, B.C. (2002b), "An extrapolation method for boundary conditions in lattice Boltzmann method", *Phys. Fluids*, Vol. 14 No. 6, pp. 2007-10.

He, X., Chen, S. and Doolen, G.D. (1998), "A novel thermal model for the lattice Boltzmann method in incompressible limit", *J. Comput. Phys.*, Vol. 146 No. 1, pp. 282-300.

Mei, R.W., Yu, D.Z., Shyy, W. and Luo, L.S. (2002), "Force evaluation in the lattice Boltzmann method involving curved geometry", *Phys. Rev. E*, Vol. 65 No. 4, p. 041203.

Mittal, S. and Kumar, B. (2003), "Flow past a rotating cylinder", *J. Fluid Mech.*, Vol. 476, pp. 303-34.

Nair, M.T., Sengupta, T.K. and Chauhan, US (1998), "Flow past rotating cylinders at high Reynolds numbers using higher order upwind scheme", *Comput. Fluids*, Vol. 27 No. 1, pp. 47-70.

Peng, Y., Shu, C. and Chew, Y.T. (2003), "Simplified thermal lattice Boltzmann model for incompressible thermal flows", *Phys. Rev. E*, Vol. 68 No. 2, p. 026701.

Shi, Y., Zhao, T.S. and Guo, Z.L. (2004), "Thermal lattice Bhatnagar-Gross-Krook model for flows with viscous heat dissipation in the incompressible limit", *Phys. Rev. E*, Vol. 70 No. 6, p. 066310.

Takada, N. and Tsutahara, M. (1998), "Evolution of viscous flow around a suddenly rotating circular cylinder in the lattice Boltzmann method", *Comput. Fluids*, Vol. 27 No. 7, pp. 807-28.

Teixeira, C., Chen, H.D. and Freed, D.M. (2000), "Multi-speed thermal lattice Boltzmann method stabilization via equilibrium under-relaxation", *Comput. Phys. Commun.*, Vol. 129 Nos 1/3, pp. 207-26.

Watari, M. and Tsutahara, M. (2004), "Possibility of constructing a multispeed Bhatnagar-Gross-Krook thermal model of the lattice Boltzmann method", *Phys. Rev. E*, Vol. 70 No. 1, p. 016703.

Yu, D.Z., Mei, R.W, Luo, L.S. and Wei, S. (2003), "Viscous flow computations with the method of lattice Boltzmann equation", *Prog. Aerosp. Sci.*, Vol. 39, pp. 329-67.

Corresponding author
Y.Y. Yan can be contacted at: yuying.yan@nottingham.ac.uk